Light scattering by a core–mantle spheroidal particle

Victor G. Farafonov, Nikolai V. Voshchinnikov, and Vadim V. Somsikov

A solution of the electromagnetic scattering problem for confocal coated spheroids has been obtained by the method of separation of variables in a spheroidal coordinate system. The main features of the solution are (i) the incident, scattered, and internal radiation fields are divided into two parts: an axisymmetric part independent of the azimuthal angle φ and a nonaxisymmetric part that with integration over φ gives zero; the diffraction problems for each part are solved separately; (ii) the scalar potentials of the solution are chosen in a special way: Abraham's potentials (for the axisymmetric part) and a superposition of the potentials used for spheres and infinitely long cylinders (for the nonaxisymmetric part). Such a procedure has been applied to homogeneous spheroids [Differential Equations **19,** 1765 (1983); Astrophys. Space Sci. **204,** 19, (1993)] and allows us to solve the light scattering problem for confocal spheroids with an arbitrary refractive index, size, and shape of the core or mantle. Numerical tests are described in detail. The efficiency factors have been calculated for prolate and oblate spheroids with refractive indices of $1.5 + 0.0i$, $1.5 + 0.05i$ for the core and refractive indices of $1.3 + 0.0i$, $1.3 + 0.05i$ for the mantle. The effects of the core size and particle shape as well as those of absorption in the core or mantle are examined. It is found that the efficiency factors of the coated and homogeneous spheroids with the volume-averaged refractive index are similar to first maximum.

Key words: Light scattering, nonspherical particles, inhomogeneous particles.

1. Introduction

In the last several years, significant progress in the theoretical study of light scattering by small particles has been discerned. The methods developed make it possible to calculate the optical properties of arbitrarily shaped particles with anisotropic optical properties and inclusions.[1–5] However, the major part of the numerical results deals with simple axisymmetric particles such as homogeneous spheroids or finite cylinders. Such models of particles should be useful as a solution to various problems in atmospheric and ocean optics, astrophysics, biophysics, etc. In most cases of practical interest, it is necessary to average over particle sizes and orientations. Then the computational method must be fast to get accurate numerical results for polydispersions of aligned nonspherical particles.

In this paper we present the solution to the problem of light scattering by core–mantle (two-layered) spheroidal particles, which makes it possible to consider inhomogeneous nonspherical particles with shapes that vary from needles (prolate spheroids) to disks (oblate spheroids). The problem is solved by the method of separation of variables in a spheroidal coordinate system. This method was used to obtain a solution to the light scattering problem for spheres and infinitely long circular cylinders that are both homogeneous and core–mantle in structure.[6–9] For homogeneous spheroids, the problem was worked out by Asano and Yamamoto[10] and Farafonov.[11] In Ref. 11 the special basis for expansion of the electromagnetic fields was introduced. Numerical results[12,13] indicate that the computational efficiency of this solution is higher than that of Asano and Yamamoto.[10] Here, similar ideas are used to solve the light scattering problem for core–mantle spheroids.

Note that core–mantle spheroids have been previously considered by Onaka[14] who extended the approach of Asano and Yamamoto.[10] Some results were published in Ref. 14 for dielectric particles with refractive indices $\tilde{m}_{\text{core}} = 1.66 + 0.0i$ and $\tilde{m}_{\text{mantle}} =$

V. G. Farafonov is with the St. Petersburg State Academy of Aerocosmic Instrumentation, St. Petersburg 190000, Russian Federation. N. V. Voshchinnikov is with the Astronomical Institute, St. Petersburg University, St. Petersburg 198904, Russian Federation. V. V. Somsikov is with the Pulkovo Observatory, St. Petersburg 196140, Russian Federation.

Received 10 May 1995; revised manuscript received 27 February 1996.

0003-6935/96/275412-15$10.00/0

1.33 + 0.0i. Cooray and Ciric[15] studied the phase function and radar cross sections for prolate layered spheroids. Their solution is based on the method of separation of variables developed by Sinha and MacPhie[16] for conducting spheroids. Coated spheroids have also been considered in Refs. 17 and 18 where the extended boundary conditions (T-matrix) method was applied. The results were done for small atmospheric and biological particles. Some calculations of the optical properties of optically soft core–mantle spheroids were made on the basis of the Rayleigh–Hans–Debye approximation (see the discussion in Ref. 19).

2. Formulation of the Problem

The problem of electromagnetic light scattering by a core–mantle particle can be solved in the prolate and oblate spheroidal coordinate systems (ξ, η, φ) that are connected with the Cartesian system (x, y, z) in the following way[20,21]:

$$x = \frac{d}{2}(\xi^2 \mp 1)^{1/2}(1 - \eta^2)^{1/2}\cos\varphi,$$

$$y = \frac{d}{2}(\xi^2 \mp 1)^{1/2}(1 - \eta^2)^{1/2}\sin\varphi,$$

$$z = \frac{d}{2}\xi\eta, \tag{1}$$

where $\xi \in [1, \infty)$, $\eta \in [-1, 1]$, and $\varphi \in [0, 2\pi)$ for a prolate coordinate system and $\xi \in [0, \infty)$, $\eta \in [-1, 1]$, and $\varphi \in [0, 2\pi)$ for an oblate coordinate system; d is the focal distance. The upper sign corresponds to the prolate system and the lower to the oblate system. Note that the confocal spheroids correspond only to the same spheroidal system. Then the thickness of the coating is variable.

Let the time-dependent part of the electromagnetic field be $\exp(-i\omega t)$ and $\mathbf{E}^{(i)}$, $\mathbf{H}^{(i)}$ and $E_\tau^{(i)}$, $H_\tau^{(i)}$ be the vectors of the electric and magnetic fields and their tangential components, respectively. The subscript i takes a value of 0, 1, 2, or 3, which refer to the field of the incident radiation, the field of the scattered radiation, and the radiation fields inside the mantle and the core of a particle. Then the scattering problem is formulated as follows (i = 1, 2, 3):

$$\nabla^2\mathbf{E}^{(i)} + k_i^2\mathbf{E}^{(i)} = 0, \tag{2}$$

$$\nabla\mathbf{E}^{(i)} = 0, \tag{3}$$

$$\left.\begin{aligned} E_\tau^{(0)} + E_\tau^{(1)} &= E_\tau^{(2)} \\ H_\tau^{(0)} + H_\tau^{(1)} &= H_\tau^{(2)} \end{aligned}\right\}_{\xi=\xi_1}, \tag{4}$$

$$\left.\begin{aligned} E_\tau^{(2)} &= E_\tau^{(3)} \\ H_\tau^{(2)} &= H_\tau^{(3)} \end{aligned}\right\}_{\xi=\xi_2}, \tag{5}$$

$$\lim_{r\to\infty} r\left(\frac{\partial\mathbf{E}^{(1)}}{\partial r} - ik_1\mathbf{E}^{(1)}\right) = 0, \tag{6}$$

where $k_i = \sqrt{\varepsilon_i\mu_i}k_0$ is the wave number in a medium with complex permittivity ε_i and magnetic permeability μ_i, $k_0 = 2\pi/\lambda_0$ is the wave number in vacuum, $\mathbf{r}$ is the radius vector, ξ_1 and ξ_2 are the radial coordinate values at the surfaces of the mantle and the core, respectively. The magnetic fields can be obtained from electrical fields using Maxwell's equations

$$\mathbf{H} = \frac{1}{i\mu k_0}\nabla\times\mathbf{E}, \quad \mathbf{E} = -\frac{1}{i\varepsilon k_0}\nabla\times\mathbf{H}.$$

We consider a plane electromagnetic wave with an arbitrary polarization propagating at an incident angle α to the rotational axis of a spheroid (or the z axis; see Fig. 1). This wave can be represented as a superposition of two components:

(a) TE mode

$$\mathbf{E}^{(0)} = -\mathbf{i}_y\exp[ik_1(x\sin\alpha + z\cos\alpha)],$$

$$\mathbf{H}^{(0)} = \sqrt{\frac{\varepsilon_1}{\mu_1}}(\mathbf{i}_x\cos\alpha - \mathbf{i}_z\sin\alpha) \times\exp[ik_1(x\sin\alpha + z\cos\alpha)]; \tag{7}$$

(b) TM mode

$$\mathbf{E}^{(0)} = (\mathbf{i}_x\cos\alpha - \mathbf{i}_z\sin\alpha)\exp[ik_1(x\sin\alpha + z\cos\alpha)],$$

$$\mathbf{H}^{(0)} = \sqrt{\frac{\varepsilon_1}{\mu_1}}\mathbf{i}_y\exp[ik_1(x\sin\alpha + z\cos\alpha)]. \tag{8}$$

Here $\mathbf{i}_x$, $\mathbf{i}_y$, $\mathbf{i}_z$ are the unit vectors in the Cartesian coordinate system.

The main features of the solution that we used are (see also Ref. 13):

(i) All the fields are divided into two parts:

$$\mathbf{E}^{(i)} = \mathbf{E}_1^{(i)} + \mathbf{E}_2^{(i)}, \quad \mathbf{H}^{(i)} = \mathbf{H}_1^{(i)} + \mathbf{H}_2^{(i)}, \quad i = 0, 1, 2, 3, \tag{9}$$

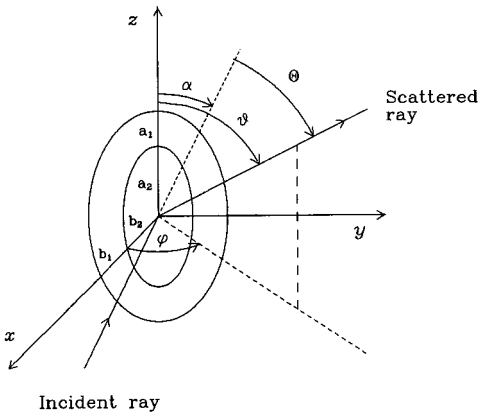

Fig. 1. Scattering geometry for a prolate spheroid with a confocal core–mantle structure. The space is divided into three parts: the outer medium, the mantle, and the core. The scattered field in the far-field zone is represented in the spherical coordinate system. The origin of the coordinate system is at the center of the spheroid whereas the z axis coincides with its axis of revolution. The angle of incidence α is the angle in the x–z plane between the direction of incidence and the z axis.

where $\mathbf{E}_1^{(i)}, \mathbf{H}_1^{(i)}$ are the axisymmetrical parts independent of the azimuthal angle φ, whereas the integration of the nonaxisymmetrical parts $\mathbf{E}_2^{(i)}$, $\mathbf{H}_2^{(i)}$ over φ gives zero.

(ii) The scalar potentials for the solution are chosen in a special way: Abraham's potentials for the axisymmetric part and the superposition of potentials used for spheres and infinitely long cylinders for the nonaxisymmetric part.

The independent solution to the first and second parts of Eqs. (9) is possible due to the commutation of the operator corresponding to the diffraction problem and the operator $L_z = \partial/\partial\varphi$ (Ref. 11). Thus, the problem under consideration can be uncoupled relative to the azimuthal angle φ, i.e., each component of Fourier expansion [including axisymmetric components $\mathbf{E}_1^{(i)}$, $\mathbf{H}_1^{(i)}$] can be found separately.

3. Solution to the Axisymmetric Problem

If the electromagnetic field does not depend on the azimuthal angle φ, we can introduce Abraham's potentials[21,22]:

$$\mathcal{P} = h_\varphi E_\varphi, \quad \mathcal{Q} = h_\varphi H_\varphi. \tag{10}$$

Using these potentials, the expressions for all the components of vectors $\mathbf{E}$ and $\mathbf{H}$ can be obtained:

$$E_\xi = -\frac{i}{k_0\varepsilon}\frac{1}{h_\eta h_\varphi}\frac{\partial\mathcal{Q}}{\partial\eta}, \quad H_\xi = \frac{i}{k_0\mu}\frac{1}{h_\eta h_\varphi}\frac{\partial\mathcal{P}}{\partial\eta},$$

$$E_\eta = \frac{i}{k_0\varepsilon}\frac{1}{h_\xi h_\varphi}\frac{\partial\mathcal{Q}}{\partial\xi}, \qquad H_\eta = -\frac{i}{k_0\mu}\frac{1}{h_\xi h_\varphi}\frac{\partial\mathcal{P}}{\partial\xi}, \tag{11}$$

where

$$h_\xi = \frac{d}{2}\left(\frac{\xi^2 \mp \eta^2}{\xi^2 \mp 1}\right)^{1/2}, \quad h_\eta = \frac{d}{2}\left(\frac{\xi^2 \mp \eta^2}{1 - \eta^2}\right)^{1/2},$$

$$h_\varphi = \frac{d}{2}\left[(\xi^2 \mp 1)(1 - \eta^2)\right]^{1/2}$$

are Lamé (metric) coefficients of the prolate (upper sign) or oblate (low sign) spheroidal coordinate system.

The azimuthal components of vectors $\mathbf{E}$ and $\mathbf{H}$ can be written using the spheroidal functions with the index $m = 1$ (Ref. 21). Let us consider a prolate spheroid. Then the components of the fields corresponding to the incident, scattered, and internal (inside the mantle and the core of the particle) radiation are

$$E_{1\varphi}^{(0)} = \sum_{l=1}^{\infty} a_l^{(0)} R_{1l}^{(1)}(c_1, \xi) S_{1l}(c_1, \eta),$$

$$H_{1\varphi}^{(0)} = \sum_{l=1}^{\infty} b_l^{(0)} R_{1l}^{(1)}(c_1, \xi) S_{1l}(c_1, \eta), \tag{12}$$

$$E_{1\varphi}^{(1)} = \sum_{l=1}^{\infty} a_l^{(1)} R_{1l}^{(3)}(c_1, \xi) S_{1l}(c_1, \eta),$$

$$H_{1\varphi}^{(1)} = \sum_{l=1}^{\infty} b_l^{(1)} R_{1l}^{(3)}(c_1, \xi) S_{1l}(c_1, \eta), \tag{13}$$

$$E_{1\varphi}^{(2)} = \sum_{l=1}^{\infty} [a_l^{(2)} R_{1l}^{(1)}(c_2, \xi) + c_l^{(2)} \times R_{1l}^{(3)}(c_2, \xi)] S_{1l}(c_2, \eta),$$

$$H_{1\varphi}^{(2)} = \sum_{l=1}^{\infty} [b_l^{(2)} R_{1l}^{(1)}(c_2, \xi) + d_l^{(2)} R_{1l}^{(3)} \times (c_2, \xi)] S_{1l}(c_2, \eta), \tag{14}$$

$$E_{1\varphi}^{(3)} = \sum_{l=1}^{\infty} a_l^{(3)} R_{1l}^{(1)}(c_3, \xi) S_{1l}(c_3, \eta),$$

$$H_{1\varphi}^{(3)} = \sum_{l=1}^{\infty} b_l^{(3)} R_{1l}^{(1)}(c_3, \xi) S_{1l}(c_3, \eta), \tag{15}$$

where $c_i = k_i d/2$ $(i = 1, 2, 3)$, $S_{ml}(c_i, \eta)$ are the prolate angular spheroidal functions with normalization coefficients $N_{ml}(c_i)$, and $R_{ml}^{(j)}(c_i, \xi)$ are the prolate radial spheroidal functions of the jth kind.[21]

The formulation of the problem [see Eqs. (2), (3), and (6)] is consistent with the fields described by Eqs. (10)–(15). One can determine the unknown coefficients $a_l^{(i)}$, $b_l^{(i)}$, $c_l^{(i)}$, and $d_l^{(i)}$ by solving the systems for the boundary conditions [Eqs. (4) and (5)] after substitution of the field expansions.

For the incident radiation we obtain the following coefficients (see Ref. 13):

(a) TE mode [Eqs. (7)]

$$a_l^{(0)} = -2i^l {N_{1l}}^{-2}(c_1) S_{1l}(c_1, \cos\alpha), \quad b_l^{(0)} = 0; \tag{16}$$

(b) TM mode [Eqs. (8)]

$$a_l^{(0)} = 0, \quad b_l^{(0)} = 2i^l \sqrt{\frac{\varepsilon_1}{\mu_1}}\, {N_{1l}}^{-2}(c_1) S_{1l}(c_1, \cos\alpha). \tag{17}$$

Equations (10) and (11) show that Abraham's potentials can be found separately from each other. Therefore, the potential $\mathcal{P}(\mathcal{Q})$ is nonzero only for the TE (TM) mode, which means that $b_l^{(1)} = b_l^{(2)} = b_l^{(3)} = d_l^{(2)} = 0$ for the TE mode and $a_l^{(1)} = a_l^{(2)} = a_l^{(3)} = c_l^{(2)} = 0$ for the TM mode.

Let us substitute Eqs. (10) and (11) into the boundary conditions [Eqs. (4) and (5)]. In the case of a TE-type wave we have

$$\left.\begin{aligned} \mathcal{P}^{(0)} + \mathcal{P}^{(1)} &= \mathcal{P}^{(2)} \\ \frac{1}{\mu_1}\frac{\partial}{\partial\xi}[\mathcal{P}^{(0)} + \mathcal{P}^{(1)}] &= \frac{1}{\mu_2}\frac{\partial}{\partial\xi}\mathcal{P}^{(2)} \end{aligned}\right\}_{\xi=\xi_1}, \tag{18}$$

$$\left.\begin{aligned} \mathcal{P}^{(2)} &= \mathcal{P}^{(3)} \\ \frac{1}{\mu_2}\frac{\partial}{\partial\xi}\mathcal{P}^{(2)} &= \frac{1}{\mu_3}\frac{\partial}{\partial\xi}\mathcal{P}^{(3)} \end{aligned}\right\}_{\xi=\xi_2}. \tag{19}$$

Now let us substitute Eqs. (12)–(15) into the expressions for radiation fields [Eqs. (18) and (19)]. The latter multiplied by ${N_{1n}}^{-1}(c_2) S_{1n}(c_2, \eta)$ and integrated over η from -1 to 1 can be rewritten in matrix

form (parameter $\tilde{f}$ is equal to 1 for the prolate spheroids and -1 for oblate spheroids):

$$\left\{\left(\frac{\mu_2}{\mu_1}-1\right)\xi_1 I+(\xi_1^{\,2}-\tilde{f})\left[\frac{\mu_2}{\mu_1}\tilde{\mathcal{R}}_3-\mathcal{R}_1(c_2,\xi_1)\right]\right\}\mathbf{Z}^{(2)}$$
$$+\left\{\left(\frac{\mu_2}{\mu_1}-1\right)\xi_1 I+(\xi_1^{\,2}-\tilde{f})\left[\frac{\mu_2}{\mu_1}\tilde{\mathcal{R}}_3-\mathcal{R}_3(c_2,\xi_1)\right]\right\}\mathbf{Y}^{(2)}$$
$$=\frac{\mu_2}{\mu_1}\Delta(c_2,c_1)(\xi_1^{\,2}-\tilde{f})[\mathcal{R}_3(c_1,\xi_1)-\mathcal{R}_1(c_1,\xi_1)]\mathbf{F}^{(0)},$$
$$\left[\left(\frac{\mu_2}{\mu_3}-1\right)\xi_2 I+(\xi_2^{\,2}-\tilde{f})\left(\frac{\mu_2}{\mu_3}\tilde{\mathcal{R}}_1-\mathcal{R}_1(c_2,\xi_2)\right)\right]P_1\mathbf{Z}^{(2)}$$
$$+\left\{\left(\frac{\mu_2}{\mu_3}-1\right)\xi_2 I+(\xi_2^{\,2}-\tilde{f})\left[\frac{\mu_2}{\mu_3}\tilde{\mathcal{R}}_3-\mathcal{R}_1(c_2,\xi_2)\right]\right\}P_3\mathbf{Y}^{(2)}=0, \tag{20}$$

where

$$\mathbf{Z}^{(j)}=\{z_l^{(j)}\}_1^{\infty},\quad \mathbf{Y}^{(2)}=\{y_l^{(2)}\}_1^{\infty},\quad \mathbf{F}^{(0)}=\{f_l^{(0)}\}_1^{\infty},$$
$$z_l^{(1)}=a_l^{(1)}R_{1l}^{(3)}(c_1,\xi_1)N_{1l}(c_1),$$
$$z_l^{(2)}=a_l^{(2)}R_{1l}^{(1)}(c_2,\xi_1)N_{1l}(c_2),$$
$$y_l^{(2)}=c_l^{(2)}R_{1l}^{(3)}(c_2,\xi_1)N_{1l}(c_2),$$
$$f_l^{(0)}=a_l^{(0)}R_{1l}^{(1)}(c_1,\xi_1)N_{1l}(c_1),$$
$$\Delta(c_i,c_j)=\{\delta_{nl}^{(m)}(c_i,c_j)\}_m^{\infty},$$
$$\mathcal{R}_j(c_i,\xi)=\{R_{ml}^{(j)'}(c_i,\xi)/R_{ml}^{(j)}(c_i,\xi)\delta_{nl}\}_m^{\infty},$$
$$P_j=P_j(c_2,\xi_1,\xi_2)=\{R_{ml}^{(j)}(c_2,\xi_2)/R_{ml}^{(j)}\times(c_2,\xi_1)\delta_{nl}\}_m^{\infty},$$
$$\tilde{\mathcal{R}}_1=\Delta(c_2,c_3)\mathcal{R}_1(c_3,\xi_2)\Delta(c_3,c_2),$$
$$\tilde{\mathcal{R}}_3=\Delta(c_2,c_1)\mathcal{R}_3(c_1,\xi_1)\Delta(c_1,c_2),$$
$$I=\{\delta_{nl}\}_m^{\infty}\text{ is the unit matrix.} \tag{21}$$

The expression for integral $\delta_{nl}^{(m)}(c_i,c_j)$ is given in the Appendix.

The coefficients $a_l^{(1)}$ that describe the scattered radiation can be used to determine the cross sections for extinction and scattering, the scattering matrix, etc. They can be found from the following equation:

$$\mathbf{Z}^{(1)}=\Delta(c_1,c_2)(\mathbf{Z}^{(2)}+\mathbf{Y}^{(2)})-\mathbf{F}^{(0)}. \tag{22}$$

For the TM mode, the transformation of the infinite system [Eqs. (20) and (21)] can be performed by the replacements $\mu_i\to\varepsilon_i$, $\varepsilon_i\to\mu_i$ and $a_l^{(j)}\to b_l^{(j)}$, $c_l^{(2)}\to d_l^{(2)}$. In order to obtain the corresponding systems for an oblate spheroid one must use the standard replacements $c\to -ic$ ($d\to -id$), $\xi\to i\xi$ and oblate spheroidal functions instead of prolate functions.

4. Solution to the Nonaxisymmetric Problem

The second terms in Eqs. (9) can be represented in the following form:

(a) TE mode

$$\mathbf{E}_2^{(i)}=\nabla\times[U^{(i)}\mathbf{i}_z+V^{(i)}\mathbf{r}],$$
$$\mathbf{H}_2^{(i)}=\frac{1}{i\mu_i k_0}\nabla\times\nabla\times[U^{(i)}\mathbf{i}_z+V^{(i)}\mathbf{r}]; \tag{23}$$

(b) TM mode

$$\mathbf{E}_2^{(i)}=-\frac{1}{i\varepsilon_i k_0}\nabla\times\nabla\times[U^{(i)}\mathbf{i}_z+V^{(i)}\mathbf{r}],$$
$$\mathbf{H}_2^{(i)}=\nabla\times[U^{(i)}\mathbf{i}_z+V^{(i)}\mathbf{r}]. \tag{24}$$

One can write the scalar potentials $U^{(i)}$ and $V^{(i)}$ using the spheroidal wave functions

$$U^{(0)}=\sum_{m=1}^{\infty}\sum_{l=m}^{\infty}a_{ml}^{(0)}R_{ml}^{(1)}(c_1,\xi)S_{ml}(c_1,\eta)\cos m\varphi,$$
$$V^{(0)}=\sum_{m=1}^{\infty}\sum_{l=m}^{\infty}b_{ml}^{(0)}R_{ml}^{(1)}(c_1,\xi)S_{ml}(c_1,\eta)\cos m\varphi, \tag{25}$$

$$U^{(1)}=\sum_{m=1}^{\infty}\sum_{l=m}^{\infty}a_{ml}^{(1)}R_{ml}^{(3)}(c_1,\xi)S_{ml}(c_1,\eta)\cos m\varphi,$$
$$V^{(1)}=\sum_{m=1}^{\infty}\sum_{l=m}^{\infty}b_{ml}^{(1)}R_{ml}^{(3)}(c_1,\xi)S_{ml}(c_1,\eta)\cos m\varphi, \tag{26}$$

$$U^{(2)}=\sum_{m=1}^{\infty}\sum_{l=m}^{\infty}[a_{ml}^{(2)}R_{ml}^{(1)}(c_2,\xi)+c_{ml}^{(2)}R_{ml}^{(3)}(c_2,\xi)]S_{ml}(c_2,\eta)\cos m\varphi,$$
$$V^{(2)}=\sum_{m=1}^{\infty}\sum_{l=m}^{\infty}[b_{ml}^{(2)}R_{ml}^{(1)}(c_2,\xi)+d_{ml}^{(2)}R_{ml}^{(3)}(c_2,\xi)]S_{ml}(c_2,\eta)\cos m\varphi, \tag{27}$$

$$U^{(3)}=\sum_{m=1}^{\infty}\sum_{l=m}^{\infty}a_{ml}^{(3)}R_{ml}^{(1)}(c_3,\xi)S_{ml}(c_3,\eta)\cos m\varphi,$$
$$V^{(3)}=\sum_{m=1}^{\infty}\sum_{l=m}^{\infty}b_{ml}^{(3)}R_{ml}^{(1)}(c_3,\xi)S_{ml}(c_3,\eta)\cos m\varphi. \tag{28}$$

For the TE mode, the coefficients that describe the incident radiation are equal to (see Ref. 13)

$$a_{ml}^{(0)}=\frac{4i^{l-1}}{k_1}N_{ml}^{-2}(c_1)\frac{S_{ml}(c_1,\cos\alpha)}{\sin\alpha},\quad b_{ml}^{(0)}=0.$$

For the TM mode, the coefficients $a_{ml}^{(0)}$ have the opposite sign and the multiplicand $\sqrt{\varepsilon_1/\mu_1}$ [see Eqs. (7), (8), (23), and (24)].

Let us introduce the vector wave functions (see Ref. 20)

$$\mathbf{M}_{ml}^{\,a}=\nabla\times(\psi_{ml}\mathbf{a}),\quad \mathbf{N}_{ml}^{\,a}=\frac{1}{k}\nabla\times\mathbf{M}_{ml}^{\,a},$$

where $\mathbf{a}$ is either the unit vector of the Cartesian system or the radius vector, ψ_{ml} are the scalar wave functions that represent the solutions to the scalar Helmholtz equation in the corresponding curvilinear coordinate system. As follows from Eqs. (23)–(28), our approach is equivalent to the choice of the vector spheroidal wave functions $\mathbf{M}_{ml}^{\,z}$, $\mathbf{N}_{ml}^{\,z}$ (i.e., $\mathbf{a}=\mathbf{i}_z$) and

$\mathbf{M}_{ml}^{r}$, $\mathbf{N}_{ml}^{r}$ (i.e., $\mathbf{a} = \mathbf{r}$) as the basic functions. Note that $\mathbf{a} = \mathbf{r}$ for spheres and $\mathbf{a} = \mathbf{i}_z$ for infinitely long cylinders.[23]

The representation of the radiation fields as described by Eqs. (23)–(28) is consistent with the formulation of the problem given by Eqs. (2), (3), and (6). The boundary conditions [Eqs. (4) and (5)] are used to find the unknown coefficients. We insert Eqs. (23) into the boundary conditions. After mathematical transformations we obtain (see Ref. 13)

$$\left.\begin{aligned}
\eta[U^{(0)} + U^{(1)}] + \frac{d}{2}\,\xi V^{(1)} &= \eta U^{(2)} + \frac{d}{2}\,\xi V^{(2)} \\
\frac{\partial}{\partial\xi}\left\{\xi[U^{(0)} + U^{(1)}] + \tilde{f}\frac{d}{2}\,\eta V^{(1)}\right\} &= \frac{\partial}{\partial\xi}\left[\xi U^{(2)} + \tilde{f}\frac{d}{2}\,\eta V^{(2)}\right] \\
\varepsilon_1\left\{\xi[U^{(0)} + U^{(1)}] + \tilde{f}\frac{d}{2}\,\eta V^{(1)}\right\} &= \varepsilon_2\left[\xi U^{(2)} + \tilde{f}\frac{d}{2}\,\eta V^{(2)}\right] \\
\frac{1}{\mu_1}\frac{\partial}{\partial\xi}\left\{\eta[U^{(0)} + U^{(1)}] + \frac{d}{2}\,\xi V^{(1)}\right\} &= \frac{1}{\mu_2}\left\{\frac{\partial}{\partial\xi}\left[\eta U^{(2)} + \frac{d}{2}\,\xi V^{(2)}\right]\right. \\
&\quad \left. + \left(1 - \frac{c_2^{\,2}}{c_1^{\,2}}\right)\frac{1-\eta^2}{\xi^2 - \tilde{f}}\frac{\partial}{\partial\eta}\left[\xi U^{(2)} + \tilde{f}\frac{d}{2}\,\eta V^{(2)}\right]\right\}
\end{aligned}\right|_{\xi=\xi_1}, \tag{29}$$

$$\left.\begin{aligned}
\eta U^{(2)} + \frac{d}{2}\,\xi V^{(2)} &= \eta U^{(3)} + \frac{d}{2}\,\xi V^{(3)} \\
\frac{\partial}{\partial\xi}\left[\xi U^{(2)} + \tilde{f}\frac{d}{2}\,\eta V^{(2)}\right] &= \frac{\partial}{\partial\xi}\left[\xi U^{(3)} + \tilde{f}\frac{d}{2}\,\eta V^{(3)}\right] \\
\varepsilon_2\left[\xi U^{(2)} + \tilde{f}\frac{d}{2}\,\eta V^{(2)}\right] &= \varepsilon_3\left[\xi U^{(3)} + \tilde{f}\frac{d}{2}\,\eta V^{(3)}\right] \\
\frac{1}{\mu_2}\left\{\frac{\partial}{\partial\xi}\left[\eta U^{(2)} + \frac{d}{2}\,\xi V^{(2)}\right] + \left(1 - \frac{c_2^{\,2}}{c_3^{\,2}}\right)\frac{1-\eta^2}{\xi^2 - f}\frac{\partial}{\partial\eta}\left[\xi U^{(2)} + \tilde{f}\frac{d}{2}\,\eta V^{(2)}\right]\right\} &= \frac{1}{\mu_3}\frac{\partial}{\partial\xi}\left[\eta U^{(3)} + \frac{d}{2}\,\xi V^{(3)}\right]
\end{aligned}\right|_{\xi=\xi_2}. \tag{30}$$

In the case of the TM mode, the analogous expressions can be obtained from Eqs. (29) and (30) by the replacements $\mu_i \to \varepsilon_i$ and $\varepsilon_i \to \mu_i$. Let us assume that $\mu_i = 1$ and $\varepsilon_1 = 1$. Then for the TM mode transformed Eqs. (29) and (30) can be written in the following form:

$$\left.\begin{aligned}
U^{(0)} + U^{(1)} &= U^{(2)} \\
\frac{\partial}{\partial\xi}\left\{\xi[U^{(0)} + U^{(1)}] + \tilde{f}\eta\,\frac{d}{2}\,V^{(1)}\right\} &= \frac{\partial}{\partial\xi}\left[\xi U^{(2)} + \tilde{f}\eta\,\frac{d}{2}\,V^{(2)}\right] \\
V^{(1)} &= V^{(2)} \\
\frac{1}{\varepsilon_1}\frac{\partial}{\partial\xi}\left\{\eta[U^{(0)} + U^{(1)}] + \frac{d}{2}\,\xi V^{(1)}\right\} &= \frac{1}{\varepsilon_2}\left\{\frac{\partial}{\partial\xi}\left[\eta U^{(2)} + \frac{d}{2}\,\xi V^{(2)}\right]\right. \\
&\quad \left. + \left(1 - \frac{c_2^{\,2}}{c_1^{\,2}}\right)\frac{1-\eta^2}{\xi^2 - \tilde{f}}\frac{\partial}{\partial\eta}\left[\xi U^{(2)} + \tilde{f}\frac{d}{2}\,\eta V^{(2)}\right]\right\}
\end{aligned}\right|_{\xi=\xi_1}, \tag{31}$$

$$
\left.
\begin{aligned}
U^{(2)} &= U^{(3)} \\
\frac{\partial}{\partial\xi}\left[\xi U^{(2)} + \tilde{f}\xi\frac{d}{2}V^{(2)}\right] &= \frac{\partial}{\partial\xi}\left[\xi U^{(3)} + \tilde{f}\xi\frac{d}{2}V^{(3)}\right] \\
V^{(2)} &= V^{(3)} \\
\frac{1}{\varepsilon_2}\left\{\frac{\partial}{\partial\xi}\left[\eta U^{(2)} + \frac{d}{2}\xi V^{(2)}\right] + \left(1 - \frac{{c_2}^2}{{c_3}^2}\right)\frac{1-\eta^2}{\xi^2 - \tilde{f}}\frac{\partial}{\partial\eta}\left[\xi U^{(2)} + \tilde{f}\frac{d}{2}\eta V^{(2)}\right]\right\} &= \frac{1}{\varepsilon_3}\frac{\partial}{\partial\xi}\left[\eta U^{(3)} + \frac{d}{2}\xi V^{(3)}\right]
\end{aligned}
\right\}_{\xi=\xi_2}. \tag{32}
$$

In addition to previous definitions [see Eqs. (21)], we introduce the following new ones:

$$
\begin{aligned}
\mathbf{Z}_j &= \{{z_{j,l}}^{(m)}\}_m^{\infty}, \qquad \mathbf{Y}_j = \{{y_{j,l}}^{(m)}\}_m^{\infty}, \\
\mathbf{X}_j &= \{{x_{j,l}}^{(m)}\}_m^{\infty}, \qquad \mathbf{F}_m = \{f_l^{(m)}\}_m^{\infty}, \\
{z_{1,l}}^{(m)} &= \kappa_1 {a_{ml}}^{(1)} {R_{ml}}^{(3)}(c_1, \xi_1) N_{ml}(c_1), \\
{z_{2,l}}^{(m)} &= c_1 {b_{ml}}^{(1)} {R_{ml}}^{(3)}(c_1, \xi_1) N_{ml}(c_1), \\
{y_{1,l}}^{(m)} &= \kappa_1 {c_{ml}}^{(2)} {R_{ml}}^{(3)}(c_2, \xi_1) N_{ml}(c_2), \\
{y_{2,l}}^{(m)} &= c_1 {d_{ml}}^{(2)} {R_{ml}}^{(3)}(c_2, \xi_1) N_{ml}(c_2), \\
{x_{1,l}}^{(m)} &= \kappa_1 {a_{ml}}^{(2)} {R_{ml}}^{(1)}(c_2, \xi_1) N_{ml}(c_2), \\
{x_{2,l}}^{(m)} &= c_1 {b_{ml}}^{(2)} {R_{ml}}^{(1)}(c_2, \xi_1) N_{ml}(c_2), \\
f_l^{(m)} &= \kappa_1 {a_{ml}}^{(0)} {R_{ml}}^{(1)}(c_1, \xi_1) N_{ml}(c_1) \\
&= 4 i^{l-1} {N_{ml}}^{-1}(c_1) \frac{S_{ml}(c_1, \cos\alpha)}{\sin\alpha} {R_{ml}}^{(1)}(c_1, \xi_1),
\end{aligned}
$$

$$
\begin{aligned}
\Gamma(c_i, c_j) &= \{{\gamma_{nl}}^{(m)}(c_i, c_j)\}_m^{\infty}, \\
K(c_i, c_j) &= \{{\kappa_{nl}}^{(m)}(c_i, c_j)\}_m^{\infty}, \\
\Sigma(c_i, c_j) &= \{{\sigma_{nl}}^{(m)}(c_i, c_j)\}_m^{\infty}.
\end{aligned} \tag{33}
$$

The expressions for the integrals on the angular spheroidal functions ${\gamma_{nl}}^{(m)}$, ${\kappa_{nl}}^{(m)}$, ${\sigma_{nl}}^{(m)}$ are given in the Appendix.

Let us substitute Eqs. (25)–(28) into Eqs. (29)–(32), then multiply them by ${N_{mn}}^{-1}(c_2) S_{mn}(c_2, \eta)\cos m\varphi$ and integrate over η from -1 to 1 and over φ from 0 to 2π. Using the orthogonality of functions $\cos m\varphi$, after some mathematical transformations (see Ref. 13), we obtain a series of systems of equations ($m = 1, 2, \ldots$):

(a) TE mode

$$
\begin{aligned}
&\left\{\xi_1[\tilde{\mathcal{R}}_3 - \mathcal{R}_1(c_2, \xi_1)] + \xi_1\left(\frac{\varepsilon_2}{\varepsilon_1} - 1\right)\mathcal{A}_3\right\}\mathbf{X}_1 + \tilde{f}\left[\Gamma[\tilde{\mathcal{R}}_3 - \mathcal{R}_1(c_2, \xi_1)] + \left(\frac{\varepsilon_2}{\varepsilon_1} - 1\right)\mathcal{A}_3\Gamma\right]\mathbf{X}_2 \\
&+ \left\{\xi_1[\tilde{\mathcal{R}}_3 - \mathcal{R}_3(c_2, \xi_1)] + \xi_1\left(\frac{\varepsilon_2}{\varepsilon_1} - 1\right)\mathcal{A}_3\right\}\mathbf{Y}_1 + \tilde{f}\left\{\Gamma[\tilde{\mathcal{R}}_3 - \mathcal{R}_3(c_2, \xi_1)] + \left(\frac{\varepsilon_2}{\varepsilon_1} - 1\right)\mathcal{A}_3\Gamma\right\}\mathbf{Y}_2 \\
&= \xi_1\Delta(c_2, c_1)[\mathcal{R}_3(c_1, \xi_1) - \mathcal{R}_1(c_1, \xi_1)]\mathbf{F}_m, \\
&\left\{\Gamma[\tilde{\mathcal{R}}_3 - \mathcal{R}_1(c_2, \xi_1)] + \xi_1\left(\frac{\varepsilon_2}{\varepsilon_1} - 1\right)\mathcal{B}_3\right\}\mathbf{X}_1 + \left\{\xi_1[\tilde{\mathcal{R}}_3 - \mathcal{R}_1(c_2, \xi_1)] + \tilde{f}\left(\frac{\varepsilon_2}{\varepsilon_1} - 1\right)\mathcal{B}_3\Gamma\right\}\mathbf{X}_2 \\
&+ \left\{\Gamma[\tilde{\mathcal{R}}_3 - \mathcal{R}_3(c_2, \xi_1)] + \xi_1\left(\frac{\varepsilon_2}{\varepsilon_1} - 1\right)\mathcal{B}_3\right\}\mathbf{Y}_1 + \left\{\xi_1[\tilde{\mathcal{R}}_3 - \mathcal{R}_3(c_2, \xi_1)] + \tilde{f}\left(\frac{\varepsilon_2}{\varepsilon_1} - 1\right)\mathcal{B}_3\Gamma\right\}\mathbf{Y}_2 \\
&= \Gamma(c_2, c_1)[\mathcal{R}_3(c_1, \xi_1) - \mathcal{R}_1(c_1, \xi_1)]\mathbf{F}_m, \\
&\left\{\xi_2[\tilde{\mathcal{R}}_1 - \mathcal{R}_1(c_2, \xi_2)] + \xi_2\left(\frac{\varepsilon_2}{\varepsilon_3} - 1\right)\mathcal{A}_1\right\}P_1\mathbf{X}_1 + \tilde{f}\left\{\Gamma[\tilde{\mathcal{R}}_1 - \mathcal{R}_1(c_2, \xi_2)]\right. \\
&\left. + \left(\frac{\varepsilon_2}{\varepsilon_3} - 1\right)\mathcal{A}_1\Gamma\right\}P_1\mathbf{X}_2 + \left\{\xi_2[\tilde{\mathcal{R}}_1 - \mathcal{R}_3(c_2, \xi_2)] + \xi_2\left(\frac{\varepsilon_2}{\varepsilon_3} - 1\right)\mathcal{A}_1\right\}P_3\mathbf{Y}_1 \\
&+ \tilde{f}\left\{\Gamma[\tilde{\mathcal{R}}_1 - \mathcal{R}_3(c_2, \xi_2)] + \left(\frac{\varepsilon_2}{\varepsilon_3} - 1\right)\mathcal{A}_1\Gamma\right\}P_3\mathbf{Y}_2 = 0, \\
&\left\{\Gamma[\tilde{\mathcal{R}}_1 - \mathcal{R}_1(c_2, \xi_2)] + \xi_2\left(\frac{\varepsilon_2}{\varepsilon_3} - 1\right)\mathcal{B}_1\right\}P_1\mathbf{X}_1 + \left\{\xi_2[\tilde{\mathcal{R}}_1 - \mathcal{R}_1(c_2, \xi_2)]\right. \\
&\left. + \tilde{f}\left(\frac{\varepsilon_2}{\varepsilon_3} - 1\right)\mathcal{B}_1\Gamma\right\}P_1\mathbf{X}_2 + \left\{\Gamma[\tilde{\mathcal{R}}_1 - \mathcal{R}_3(c_2, \xi_2)]\right. \\
&\left. + \xi_2\left(\frac{\varepsilon_2}{\varepsilon_3} - 1\right)\mathcal{B}_1\right\}P_3\mathbf{Y}_1 + \left\{\xi_2[\tilde{\mathcal{R}}_1 - \mathcal{R}_3(c_2, \xi_2)] + \tilde{f}\left(\frac{\varepsilon_2}{\varepsilon_3} - 1\right)\mathcal{B}_1\Gamma\right\}P_3\mathbf{Y}_2 = 0,
\end{aligned} \tag{34}
$$

where

$$\mathcal{A}_1 = [\xi_2(I + \xi_2\tilde{\mathcal{R}}_1) - \tilde{f}\Gamma\tilde{\mathcal{R}}_1\Gamma]\boldsymbol{Q}(c_2, \xi_2),$$
$$\mathcal{A}_3 = [\xi_1(I + \xi_1\tilde{\mathcal{R}}_3) - \tilde{f}\Gamma\tilde{\mathcal{R}}_3\Gamma]\boldsymbol{Q}(c_2, \xi_1),$$
$$\mathcal{B}_1 = [\xi_2\Gamma\tilde{\mathcal{R}}_1 - (I + \xi_2\tilde{\mathcal{R}}_1)\Gamma]\boldsymbol{Q}(c_2, \xi_2) + \frac{1}{\xi_2^{\,2} - \tilde{f}}K(c_2, c_2),$$
$$\mathcal{B}_3 = [\xi_1\Gamma\tilde{\mathcal{R}}_3 - (I + \xi_1\tilde{\mathcal{R}}_3)\Gamma]\boldsymbol{Q}(c_2, \xi_1) + \frac{1}{\xi_1^{\,2} - \tilde{f}}K(c_2, c_2),$$
$$\Gamma = \Gamma(c_2, c_2), \quad \boldsymbol{Q}(c, \xi) = [\xi^2 I - \tilde{f}\Gamma^2(c, c)]^{-1}; \tag{35}$$

(b) TM mode

$$\mathbf{Z}_2 = \Delta(c_1, c_2)\left\{\left[\frac{\varepsilon_2}{\varepsilon_1}I + \left(\frac{\varepsilon_2}{\varepsilon_1} - 1\right)\xi_1^{\,2}\boldsymbol{Q}(c_2, \xi_1)\right](\mathbf{X}_2 + \mathbf{Y}_2) - \left(\frac{\varepsilon_2}{\varepsilon_1} - 1\right)\xi_1\Gamma\boldsymbol{Q}(c_2, \xi_1)(\mathbf{X}_1 + \mathbf{Y}_1)\right\}; \tag{37}$$

(b) TM mode

$$\mathbf{Z}_1 = \Delta(c_1, c_2)(\mathbf{X}_1 + \mathbf{Y}_1) - \mathbf{F}_m, \quad \mathbf{Z}_2 = \Delta(c_1, c_2)(\mathbf{X}_2 + \mathbf{Y}_2). \tag{38}$$

If we turn to the spherical particles [$\xi_1 > \xi_2 \to \infty$, $d \to 0$, and $\xi_1 \cdot (d/2) = r_1$, $\xi_2 \cdot (d/2) = r_2$ are the radii of confocal spheres], then the systems of equations give the exact solution. Its difference from the standard Mie solution is in the choice of distinct scalar potentials and the uncomfortable coordinate system with the z axis not coinciding with the direction of the propagation of the plane wave.

The proposed solution allows us to investigate analytically the systems of the linear algebraic equations and the convergence of the expansions for the internal and scattered radiation fields. The final-

$$\begin{aligned}
&\xi_1[\tilde{\mathcal{R}}_3 - \mathcal{R}_1(c_2, \xi_1)]\mathbf{X}_1 + \tilde{f}\Gamma[\tilde{\mathcal{R}}_3 - \mathcal{R}_1(c_2, \xi_1)]\mathbf{X}_2 \\
&+ \xi_1[\tilde{\mathcal{R}}_3 - \mathcal{R}_3(c_2, \xi_1)]\mathbf{Y}_1 + \tilde{f}\Gamma[\tilde{\mathcal{R}}_3 - \mathcal{R}_3(c_2, \xi_1)]\mathbf{Y}_2 \\
&= \xi_1\Delta(c_2, c_1)[\mathcal{R}_3(c_1, \xi_1) - \mathcal{R}_1(c_1, \xi_1)]\mathbf{F}_m, \\
&\left\{\Gamma[\tilde{\mathcal{R}}_3 - \mathcal{R}_1(c_2, \xi_1)] + \left(\frac{\varepsilon_2}{\varepsilon_1} - 1\right)\left[\Gamma\tilde{\mathcal{R}}_3 + \frac{\xi_1}{\xi_1^{\,2} - \tilde{f}}K(c_2, c_2)\right]\right\}\mathbf{X}_1 \\
&+ \left\{\xi_1[\tilde{\mathcal{R}}_3 - \mathcal{R}_1(c_2, \xi_1)] + \left(\frac{\varepsilon_2}{\varepsilon_1} - 1\right)\left[I + \xi_1\tilde{\mathcal{R}}_3 + \frac{\tilde{f}}{\xi_1^{\,2} - \tilde{f}}\Sigma(c_2, c_2)\right]\right\}\mathbf{X}_2 \\
&+ \left\{\Gamma[\tilde{\mathcal{R}}_3 - \mathcal{R}_3(c_2, \xi_1)] + \left(\frac{\varepsilon_2}{\varepsilon_1} - 1\right)\left[\Gamma\tilde{\mathcal{R}}_3 + \frac{\xi_1}{\xi_1^{\,2} - \tilde{f}}K(c_2, c_2)\right]\right\}\mathbf{Y}_1 \\
&+ \left\{\xi_1[\tilde{\mathcal{R}}_3 - \mathcal{R}_3(c_2, \xi_1)] + \left(\frac{\varepsilon_2}{\varepsilon_1} - 1\right)\left[I + \xi_1\tilde{\mathcal{R}}_3 + \frac{\tilde{f}}{\xi_1^{\,2} - \tilde{f}}\Sigma(c_2, c_2)\right]\right\}\mathbf{Y_2} \\
&= \frac{\boldsymbol{\varepsilon_2}}{\boldsymbol{\varepsilon_1}}\boldsymbol{\Gamma(c_2, c_1)}[\mathcal{R}_3(\mathbf{c_1}, \boldsymbol{\xi_1}) - \mathcal{R}_1(\mathbf{c_1}, \boldsymbol{\xi_1})]\mathbf{F}_m, \\
&\xi_2[\tilde{\mathcal{R}}_1 - \mathcal{R}_1(c_2, \xi_2)]P_1\mathbf{X}_1 + \tilde{f}\Gamma[\tilde{\mathcal{R}}_1 - \mathcal{R}_1(c_2, \xi_2)]P_1\mathbf{X}_2 \\
&+ \xi_2[\tilde{\mathcal{R}}_1 - \mathcal{R}_3(c_2, \xi_2)]P_3\mathbf{Y}_1 + \tilde{f}\Gamma[\tilde{\mathcal{R}}_1 - \mathcal{R}_3(c_2, \xi_2)]P_3\mathbf{Y}_2 = 0, \\
&\left\{\Gamma[\tilde{\mathcal{R}}_1 - \mathcal{R}_1(c_2, \xi_2)] + \left(\frac{\varepsilon_2}{\varepsilon_3} - 1\right)\left[\Gamma\tilde{\mathcal{R}}_1 + \frac{\xi_2}{\xi_2^{\,2} - \tilde{f}}K(c_2, c_2)\right]\right\}P_1\mathbf{X}_1 \\
&+ \left\{\xi_2[\tilde{\mathcal{R}}_1 - \mathcal{R}_1(c_2, \xi_2)] + \left(\frac{\varepsilon_2}{\varepsilon_3} - 1\right)\left[I + \xi_2\tilde{\mathcal{R}}_1 + \frac{\tilde{f}}{\xi_2^{\,2} - \tilde{f}}\Sigma(c_2, c_2)\right]\right\}P_1\mathbf{X}_2 \\
&+ \left\{\Gamma[\tilde{\mathcal{R}}_1 - \mathcal{R}_3(c_2, \xi_2)] + \left(\frac{\varepsilon_2}{\varepsilon_3} - 1\right)\left[\Gamma\tilde{\mathcal{R}}_1 + \frac{\xi_2}{\xi_2^{\,2} - \tilde{f}}K(c_2, c_2)\right]\right\}P_3\mathbf{Y}_1 \\
&+ \left\{\xi_2[\tilde{\mathcal{R}}_1 - \mathcal{R}_3(c_2, \xi_2)] + \left(\frac{\varepsilon_2}{\varepsilon_3} - 1\right)\left[I + \xi_2\tilde{\mathcal{R}}_1 + \frac{\tilde{f}}{\xi_2^{\,2} - \tilde{f}}\Sigma(c_2, c_2)\right]\right\}P_3\mathbf{Y}_2 = 0.
\end{aligned} \tag{36}$$

The coefficients for the field of the scattered radiation can be found from the following expressions:

(a) TE mode

$$\mathbf{Z}_1 = \Delta(c_1, c_2)\left\{\left[I + \left(\frac{\varepsilon_2}{\varepsilon_1} - 1\right)\xi_1^{\,2}\boldsymbol{Q}(c_2, \xi_1)\right](\mathbf{X}_1 + \mathbf{Y}_1) + \tilde{f}\left(\frac{\varepsilon_2}{\varepsilon_1} - 1\right)\xi_1\Gamma\boldsymbol{Q}(c_2, \xi_1)(\mathbf{X}_2 + \mathbf{Y}_2)\right\} - \mathbf{F}_m,$$

conclusions for core–mantle spheroids coincide with those for homogeneous spheroids (see the discussion in Ref. 11). The main ideas can be briefly described as follows.

Let us consider an arbitrary prolate or oblate spheroid that does not degenerate into a needle ($\xi_1 = 1$ for the prolate spheroidal coordinate system) or a disk ($\xi_1 = 0$ for the oblate system). Using the asymptotic expansions for spheroidal functions and integrals $\delta_{nl}^{(m)}$, $\gamma_{nl}^{(m)}$, etc. in the case of large indices l and n, the systems of linear algebraic equations [Eqs. (20), (34), and (36)] can be transformed into the following form:

$$z_n = \beta_1 z_{n+1} + \beta_2 z_{n-1} + \sum_{i=1}^{\infty} g_{ni} z_i + f_n, \qquad (39)$$

where $n = 1, 2, \ldots, z_0 = 0$ and

$$|\beta_1| + |\beta_2| \le p < 1, \quad \sum_{i=1}^{\infty} |g_{ni}| \le \text{const}/n, \quad \sum_{n=1}^{\infty} |f_n|^2 < \infty.$$

These systems are quasi-regular, i.e., the sum of the absolute values of coefficients on the right-hand side of Eq. (39) becomes smaller than unity beginning from some number $n > \tilde{N}$:

$$|\beta_1| + |\beta_2| + \sum_{i=1}^{\infty} |g_{ni}| \le \tilde{p} < 1.$$

The systems given by Eq. (39) have a unique solution in space l_2 (i.e., $\sum_{n=1}^{\infty} |z_n|^2 < \infty$), which can be determined by the reduction method (this means that we can solve the truncated systems). The obtained field of the scattered radiation [see Eqs. (13) and (26)] belongs to the space $L_2(S)$, where S is the surface of a confocal spheroid larger than or equal to the given one.

Asano[24] and Barber[25] indicated that the solution of Asano and Yamomoto and the T-matrix method lead to the numerical instability that occurs when one solves the system of linear equations for the axisymmetric part when $c \ge 17$. For the T-matrix method it has been shown that the use of extended precision in the calculations permits enlargement of the limits to some extent.[26] In the approach described, such a defect is absent because Eqs. (20) can be rewritten as Eq. (39) but with the coefficients $\beta_1 = \beta_2 = 0$.

5. Characteristics of Scattered Radiation

Let us assume that the incident radiation propagates in the x–z plane of the Cartesian coordinate system, the scattering plane contains the Oz axis (the rotational axis of a spheroid), and the wave vector of scattered radiation (see Fig. 1). The relation between the fields of the incident and scattered radiation is determined by the amplitude matrix

$$\begin{pmatrix} E_{\parallel}^{(1)} \\ E_{\perp}^{(1)} \end{pmatrix} = \frac{1}{-ik_1 r} \exp[i(k_1 r - \mathbf{k}_1 \mathbf{r})] \begin{pmatrix} T_{22} & T_{12} \\ T_{21} & T_{11} \end{pmatrix} \begin{pmatrix} E_{\parallel}^{(0)} \\ E_{\perp}^{(0)} \end{pmatrix}, \qquad (40)$$

where the subscripts of the dimensionless intensity functions T_{ij} are made in accordance with the rule: the first (or second) index denotes the polarization of an incident (or scattered) wave. If it is equal to 1 (or 2), the electric vector of the beam is perpendicular (or parallel) to the corresponding reference plane.

In the far zone [$r \to \infty$ in the spherical coordinate system (r, ϑ, φ) or $\xi \to \infty$, $\eta \to \cos\vartheta$, $\mathbf{i}_\eta \to -\mathbf{i}_\vartheta$ in the spheroidal system], we obtain (see Ref. 13)

$$T_{11} = \sum_{l=1}^{\infty} i^{-l} a_l^{(1)} S_{1l}(c_1, \cos\vartheta) - \sum_{m=1}^{\infty} \sum_{l=m}^{\infty} i^{-(l-1)} \times [k_1 a_{ml}^{(1)} S_{ml}(c_1, \cos\vartheta) + i b_{ml}^{(1)} S'_{ml}(c_1, \cos\vartheta)] \sin\vartheta \cos m\varphi, \qquad (41)$$

$$T_{12} = \sum_{m=1}^{\infty} \sum_{l=m}^{\infty} i^{-l} b_{ml}^{(1)} \frac{m S_{ml}(c_1, \cos\vartheta)}{\sin\vartheta} \sin m\varphi, \qquad (42)$$

$$T_{21} = \sum_{m=1}^{\infty} \sum_{l=m}^{\infty} i^{-l} b_{ml}^{(1)} \frac{m S_{ml}(c_1, \cos\vartheta)}{\sin\vartheta} \sin m\varphi, \qquad (43)$$

$$T_{22} = -\sum_{l=1}^{\infty} i^{-l} b_l^{(1)} S_{1l}(c_1, \cos\vartheta) + \sum_{m=1}^{\infty} \sum_{l=m}^{\infty} i^{-(l-1)} \times [k_1 a_{ml}^{(1)} S_{ml}(c_1, \cos\vartheta) + i b_{ml}^{(1)} S'_{ml}(c_1, \cos\vartheta)] \sin\vartheta \cos m\varphi. \qquad (44)$$

Using the amplitude matrix, we can find the scattering matrix[27] that allows us to combine the Stokes parameters of incident radiation with the scattered radiation, which gives complete information about scattered radiation. Elements of the scattering matrix are not the amplitude functions, but the products of them, the so-called dimensionless intensity functions of scattered radiation $i_{ij} = |T_{ij}|^2$.

If the incident radiation is nonpolarized, the intensity of scattered radiation can be calculated according to the formula $i(\vartheta, \varphi) = \frac{1}{2}(i_{11} + i_{12} + i_{21} + i_{22})$. The integral characteristics of scattered radiation (cross sections of a particle for extinction C_{ext}, scattering C_{sca}, and absorption C_{abs}) are determined as[27]

$$C_{\text{ext}} = \frac{4\pi}{k_1^2} \text{Re}[\mathbf{A}^{(1)}, \mathbf{i}^{(0)}]|_{\Theta=0^\circ}, \qquad (45)$$

$$C_{\text{sca}} = \frac{1}{k_1^2} \int_{4\pi} \int |\mathbf{A}^{(1)}|^2 d\Omega, \qquad (46)$$

$$C_{\text{abs}} = C_{\text{ext}} - C_{\text{sca}}, \qquad (47)$$

where $\mathbf{A}^{(1)}$ is the amplitude of the electrical field for scattered radiation, $\mathbf{i}^{(0)}$ is the unit vector that defines the polarization of incident radiation, $d\Omega$ is an element of the solid angle, and Θ is the scattering angle (angle between the directions of the incident and scattered waves). The angle Θ is connected with angles α, ϑ, and φ by the relation $\cos\Theta = \cos\alpha \cos\vartheta + \sin\alpha \sin\vartheta \cos\varphi$.

Equations (41)–(47) can be used to compute various cross sections that are usually normalized by the viewing geometric cross section of a spheroid (the

area of the particle shadow):

$$G(\alpha) = \pi b_1(a_1^2 \sin^2 \alpha + b_1^2 \cos^2 \alpha)^{1/2} \quad \text{for a prolate spheroid,} \quad (48)$$

$$G(\alpha) = \pi a_1(a_1^2 \cos^2 \alpha + b_1^2 \sin^2 \alpha)^{1/2} \quad \text{for an oblate spheroid,} \quad (49)$$

where a_1 and b_1 are the major and minor semiaxes of a coated spheroid. Then the corresponding efficiency factors $Q = C/G$ can be written as follows:

$$Q_{\text{ext}} = \frac{4}{c_1^2[(\xi_1^2 - \tilde{f})(\xi_1^2 - \tilde{f}\cos^2 \alpha)]^{1/2}} \times \text{Re}\left\{-\sum_{l=1}^{\infty} i^{-l} a_l^{(1)} S_{1l}(c_1, \cos \alpha) + \sum_{m=1}^{\infty}\sum_{l=m}^{\infty} i^{-(l-1)}[k_1 a_{ml}^{(1)} S_{ml}(c_1, \cos \alpha) + i b_{ml}^{(1)} S'_{ml}(c_1, \cos \alpha)]\sin \alpha\right\}, \quad (50)$$

$$Q_{\text{sca}} = \frac{1}{c_1^2[(\xi_1^2 - \tilde{f})(\xi_1^2 - \tilde{f}\cos^2 \alpha)]^{1/2}} \times \left\{2\sum_{l=1}^{\infty} |a_l^{(1)}|^2 N_{1l}^2(c_1) + \text{Re}\sum_{m=1}^{\infty}\sum_{l=m}^{\infty}\sum_{n=m}^{\infty} i^{n-l} \times \{k_1^2 a_{ml}^{(1)} a_{mn}^{(1)*} \omega_{ln}^{(m)}(c_1, c_1) + ik_1[b_{ml}^{(1)} a_{mn}^{(1)*} \kappa_{ln}^{(m)}(c_1, c_1) - a_{ml}^{(1)} b_{mn}^{(1)*} \kappa_{nl}^{(m)}(c_1, c_1)] + b_{ml}^{(1)} b_{mn}^{(1)*} \tau_{ln}^{(m)}(c_1, c_1)\} N_{ml}(c_1) N_{mn}(c_1)\right\}, \quad (51)$$

where $\omega_{ln}^{(m)}$, $\kappa_{ln}^{(m)}$, and $\tau_{ln}^{(m)}$ are the integrals of angular spheroidal functions (see the Appendix), the asterisk denotes the complex conjugation. Equations (50) and (51) are valid for TE and TM polarization of incident radiation but for the TM mode the coefficients $a_l^{(1)}$ should be replaced by coefficients $b_l^{(1)}$, whereas the coefficients $a_{ml}^{(1)}$ and $b_{ml}^{(1)}$ can be determined from Eqs. (36) and (38).

To compare the optical properties of particles of various shape, the cross sections can be normalized by the geometric cross section of the equivolume sphere

$$\frac{C}{\pi r_{v_1}^2} = \frac{(\xi_1^2 - \tilde{f}\cos^2 \alpha)^{1/2}}{[\xi_1^4(\xi_1^2 - \tilde{f})]^{1/6}} Q. \quad (52)$$

Here, r_{v_1} is the radius of the sphere with the volume equal to that of a given spheroidal particle and, as above, $\tilde{f} = 1$ for prolate spheroids and $\tilde{f} = -1$ for oblate spheroids. The radius of the equivolume sphere can be defined as

$$r_{v_{1,2}}^3 = a_{1,2} b_{1,2}^2 \quad \text{for prolate spheroids,} \quad (53)$$

$$r_{v_{1,2}}^3 = a_{1,2}^2 b_{1,2} \quad \text{for oblate spheroids} \quad (54)$$

where a_2 and b_2 are the major and minor semiaxes of the core.

The radial coordinates ξ_2 and ξ_1 that define the inner and outer boundaries of a spheroidal particle (surface of the core and mantle) are connected with the corresponding semiaxes as

$$\xi_{1,2} = \frac{a_{1,2}}{b_{1,2}}\left[\left(\frac{a_{1,2}}{b_{1,2}}\right)^2 - 1\right]^{-1/2} \quad \text{for a prolate spheroid,} \quad (55)$$

$$\xi_{1,2} = \left[\left(\frac{a_{1,2}}{b_{1,2}}\right)^2 - 1\right]^{-1/2} \quad \text{for an oblate spheroid.} \quad (56)$$

The efficiency factors can also be considered as a function of size parameter $2\pi a_1/\lambda$ given by

$$\frac{2\pi a_1}{\lambda} = c_1 \xi_1 \quad \text{for a prolate spheroid,} \quad (57)$$

$$\frac{2\pi a_1}{\lambda} = c_1(\xi_1^2 + 1)^{1/2} \quad \text{for an oblate spheroid.} \quad (58)$$

In some cases it is useful to know the ratio of the core-to-mantle volume or the core volume to the total volume of a coated particle. For confocal spheroids, one can determine the latter ratio using the semiaxes ratios or parameters ξ_1 and ξ_2 as

$$\frac{V_{\text{core}}}{V_{\text{total}}} = \frac{\xi_2(\xi_2^2 - \tilde{f})}{\xi_1(\xi_1^2 - \tilde{f})}. \quad (59)$$

Equation (59) also allows us to calculate the values of ξ_1 or ξ_2 when the ratio $V_{\text{core}}/V_{\text{total}}$ is the input parameter. For a prolate spheroid, the iterative scheme can be applied in the following manner:

$$(\xi_{1,2})^{(n)} = \left[(\xi_{1,2})^{(n-1)} + \frac{V_{\text{total,core}}}{V_{\text{core,total}}} \xi_{2,1}(\xi_{2,1}^2 - 1)\right]^{1/3}, \quad (60)$$

where $n = 1, 2 \ldots$ and the initial value $(\xi_{1,2})^{(0)} = \xi_{2,1}$. For an oblate spheroid, parameter $\xi_{1,2}$ can be found using Newton's method

$$(\xi_{1,2})^{(n)} = \frac{2[(\xi_{1,2})^{(n-1)}]^3 + \frac{V_{\text{total,core}}}{V_{\text{core,total}}} \xi_{2,1}(\xi_{2,1}^2 + 1)}{3[(\xi_{1,2})^{(n-1)}]^2 + 1}, \quad (61)$$

where $n = 1, 2 \ldots$ and the initial value $(\xi_{1,2})^{(0)} = 0$.

The thickness of the mantle τ is not constant across the surface of a confocal coated spheroid. For a ray with incident angle α, τ is equal to

$$\tau = a_1\left[\left(\frac{a_1}{b_1}\right)^2 \sin^2 \alpha + \cos^2 \alpha\right]^{-1/2} - a_2\left[\left(\frac{a_2}{b_2}\right)^2 \sin^2 \alpha + \cos^2 \alpha\right]^{-1/2} \quad (62)$$

Table 1. Efficiency Factors for Extinction Q_{ext} and Scattering Q_{sca} for Core–Mantle Spheres and Spheroids at $\alpha = 0°$ [a]

	Sphere	Prolate Spheroid				Oblate Spheroid			
		$a_1/b_1 = 2$		$a_1/b_1 = 10$		$a_1/b_1 = 2$		$a_1/b_1 = 10$	
N	Q_{sca}	Q_{ext}	Q_{sca}	Q_{ext}	Q_{sca}	Q_{ext}	Q_{sca}	Q_{ext}	Q_{sca}
4	1.09	4.15	4.03	0.232	0.219	1.84	2.56	0.185	0.178
6	3.638	6.419	6.445	0.224	0.221	1.608	1.629	0.162	0.169
8	3.5801	6.4163	6.4156	0.2250	0.2252	1.6369	1.6365	0.1637	0.1636
10	3.57777	6.41811	6.41812	0.22445	0.22444	1.63663	1.63664	0.163724	0.163724
12	3.577749	6.418088	6.418088	0.224454	0.224454	1.636630	1.636630	0.163729	0.163728
14	3.577749	6.418089	6.418089	0.224454	0.224454	1.636630	1.636630	0.163729	0.163729

[a] $\tilde{m}_{core} = 1.5 + 0.0i$, $\tilde{m}_{mantle} = 1.3 + 0.0i$, $2\pi a_1/\lambda = 5$, and $V_{core}/V_{total} = 0.5$.

for a prolate spheroid and

$$\tau = a_1\left[\left(\frac{a_1}{b_1}\right)^2 \cos^2\alpha + \sin^2\alpha\right]^{-1/2} - a_2\left[\left(\frac{a_2}{b_2}\right)^2 \cos^2\alpha + \sin^2\alpha\right]^{-1/2} \quad (63)$$

for an oblate spheroid.

6. Computational Tests

The numerical code for coated spheroids is based on a previous code for homogeneous particles (see Ref. 13). The restrictions for large particles are mainly the result of calculation difficulties with the spheroidal functions. This problem is divided into two parts: determination of the eigenvalues and a reasonable choice of the method for spheroidal function expansion. At present, an exact and effective method for determination of eigenvalues has been developed. It appears to have no restrictions and can be used to calculate the eigenvalues with parameter c as high as 100. For calculation of spheroidal functions, we use the expansions in terms of Legendre functions, Bessel functions, or solutions of the corresponding differential equations, depending on the size and shape of a particle. The computational program was examined using various tests, which included internal control as well as a comparison with known results for homogeneous spheroids and core–mantle spheres.

(1) For nonabsorbing particles the efficiency factors for extinction and scattering must be equal for the same azimuthal index m: $Q_{ext}^{(m)} = Q_{sca}^{(m)}[Q = \sum_m Q^{(m)}]$. Then by increasing the number of terms N in sums over l and n [Eqs. (50) and (51)], one should obtain the decreasing difference between these two factors, i.e., $|Q_{ext}^{(m)} - Q_{sca}^{(m)}| \to 0$ if $N \to \infty$. Table 1 shows the behavior of efficiency factors in the case of radiation propagating along the rotation axis of a spheroid when the sums over m contain only one term for $m = 1$. Our calculations demonstrate that the convergence for spheroids follows that for core–mantle spheres. The efficiency factors for core–mantle spheres have been calculated using the method from Ref. 28. The convergence can be determined by the particle size $2\pi a_1/\lambda$ and is independent of its shape. The latter is explained by the successful choice of scalar potentials. Note that Asano and Yamomoto[10] used Debye's potentials that requires one to increase considerably the number of terms N for extremely prolate or oblate particles.

(2) The values of the efficiency factors for TM and TE polarization are the same as for parallel radiation incidence (i.e., if $\alpha = 0°$). This test is not trivial since one can carry out the calculations using different expressions for each mode.

(3) When summing over the azimuthal index m in Eqs. (50) and (51), the convergence of efficiency factors should also occur. This is shown in Table 2 for radiation that propagates perpendicular to the rotation axis of a spheroid. It can be seen how the convergence process depends on particle shape. In reality, the number of terms M correlates with the volume of a particle that is proportional to parameters c_1 and ξ_1 (i.e., the volume grows with a decrease of the ratio a_1/b_1). Note that, as follows from Eqs. (53)–(58), for the same values of c_1 and a_1/b_1 the volume of the oblate particle is a_1/b_1 times larger than that of a prolate particle.

(4) A detailed comparison of the optical properties of core–mantle and homogeneous spheroids has been made using different transformations of a core–mantle particle to a homogeneous particle: (i) $V_{core}/V_{total} \to 0$, (ii) $V_{core}/V_{total} \to 1$, (iii) $\tilde{m}_{core} = \tilde{m}_{mantle}$, (iv) $\tilde{m}_{mantle} = 1.0 + 0.0i$. In all cases we found that the factors for core–mantle particles became closer to those for spheroids consisting of the core or mantle material only.

Table 2. Efficiency Factors for Scattering Q_{sca} for Core–Mantle Spheroids[a]

	Prolate Spheroid		Oblate Spheroid	
M	$a_1/b_1 = 2$	$a_1/b_1 = 10$	$a_1/b_1 = 2$	$a_1/b_1 = 10$
1	1.702229	0.04962866	2.152832	0.2755930
2	1.808355	0.04962866	3.317797	0.3845179
3	1.808948	—	4.503349	0.4001552
4	1.808949	—	4.670039	0.4008675
5	1.808949	—	4.673185	0.4008813
6	—	—	4.673225	0.4008815
7	—	—	4.673225	0.4008815

[a] $\tilde{m}_{core} = 1.5 + 0.0i$, $\tilde{m}_{mantle} = 1.3 + 0.0i$, $c_1 = 4$, $\alpha = 90°$, and $V_{core}/V_{total} = 0.5$.

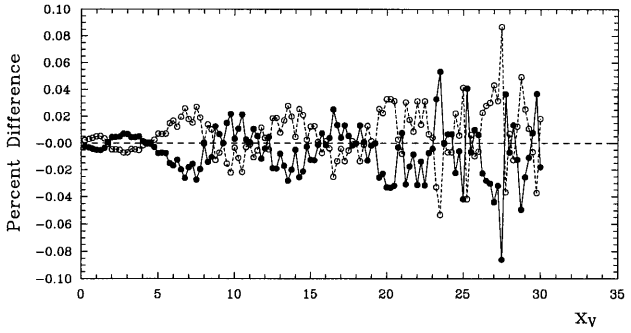

Fig. 2. Percent difference between coated spheres and coated spheroids ϵ defined by Eq. (64): $\tilde{m}_{\text{core}} = 1.5 + 0.0i$, $\tilde{m}_{\text{mantle}} = 1.3 + 0.0i$, $V_{\text{core}}/V_{\text{total}} = 0.5$, $a_1/b_1 = 1.0001$, ●, prolate spheroids, ○, oblate spheroids.

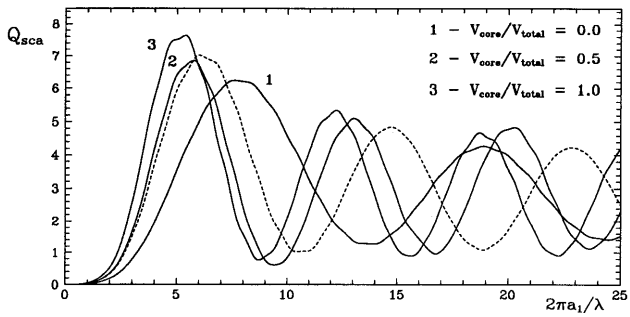

Fig. 3. Scattering efficiency factors Q_{sca} at $\alpha = 0°$ as a function of size parameter $2\pi a_1/\lambda$ for the prolate coated spheroids (solid curves): $\tilde{m}_{\text{core}} = 1.5 + 0.0i$, $\tilde{m}_{\text{mantle}} = 1.3 + 0.0i$, $a_1/b_1 = 2$. The dashed curve represents the results for homogeneous spheroids with $\tilde{m} = 1.4 + 0.0i$.

(5) When particles are nearly spherical, the optical properties of coated spheroids and core–mantle spheres should be almost the same. We considered various absorbing and dielectric particles. Some results for nonabsorbing particles are shown in Fig. 2 where we present the relative differences in percent:

$$\epsilon = \frac{Q_{\text{sca}}(\text{sphere}) - C_{\text{sca}}(\text{spheroid})/\pi r_v^{\,2}}{Q_{\text{sca}}(\text{sphere})}\,100\%. \quad (64)$$

The values of ϵ are plotted as a function of the size parameter $x_v = 2\pi r_v/\lambda$ for spheroidal particles with an aspect ratio of $a_1/b_1 = 1.0001$ and a volume ratio of $V_{\text{core}}/V_{\text{total}} = 0.5$. Then the aspect ratio of the core is constant and equal to $a_2/b_2 \approx 1.00016$. The wavelike behavior is typical only for dielectric particles. For highly absorbing particles, the values of ϵ demonstrate smooth, monotonous growth with x_v. In the interval of the aspect ratios a_1/b_1 from 1.0001 to 1.01, the percent difference is invariant to this ratio and $|\epsilon| < 5(a_1/b_1 - 1)$ if $x_v \leq 20$–25. Note also that the behavior of percent difference is independent of the particle structure (ratio $V_{\text{core}}/V_{\text{total}}$). The difference between spheroidal and spherical particles occurs because of small deviations between their shapes. Because of the different path of radiation inside prolate and oblate spheroids [see Eqs. (62) and (63)] at parallel incidence, we obtained the interference picture in the opposite phase. When $\alpha = 90°$, the picture remains the same, but the open circles (oblate spheroids) and filled circles (prolate spheroids) exchange places.

All the calculations were performed on a PC/AT-486/50 computer. Using the last version of the numerical code[29] (January 1995), the PC requires ~1.5 min of CPU time and ~1.4 Mbytes of memory to compute the efficiency factors in Table 2 (oblate spheroids, $a_1/b_1 = 2$, $m = 1, \ldots, 7$, $N = 14$). If we also calculate the factors for the TE mode ($N = 20$), the PC needs ~4.5 min of CPU time and ~3.3 Mbytes of memory. We also found that the computational time increases proportional to $N^2 \div N^{2.5}$ and the required memory increases to N^2.

7. Numerical Results and Discussion

In this section we present the results of numerical calculations that illustrate the behavior of efficiency factors. The most intriguing feature in the case of core–mantle spheroids is the opportunity to study the influence of the particle structure (i.e., core size and shape), whereas the variations of particle shape and inclination angle α affect the optical properties in the same way as for homogeneous spheroids. However, because of the confocal structure, we cannot consider the particles with arbitrary core and mantle size and shape. To describe a core–mantle spheroid geometry, three different parameters can be used (for example, c_1, a_1/b_1, a_2/b_2 or $2\pi a_1/\lambda$, a_1/b_1, $V_{\text{core}}/V_{\text{mantle}}$). Other particle characteristics can be calculated from Eqs. (53)–(63). The principal limitation for confocal spheroids is that $a_2/b_2 > a_1/b_1$, which means that we can consider particles with a nonspherical core and an almost spherical mantle but not vice versa. Nevertheless, the remaining space of possible parameter values enlarges considerably the well-studied models of core–mantle spheres and infinitely long cylinders.

Below we discuss some results for prolate and oblate spheroids with $a_1/b_1 = 2$ and 10. If we fix the values of $V_{\text{core}}/V_{\text{mantle}}$ and a_1/b_1, then the shape of the core remains the same for all particle sizes $2\pi a_1/\lambda$. For $V_{\text{core}}/V_{\text{mantle}} = 0.5$ and $a_1/b_1 = 2$ (or 10), the core aspect ratio is equal to $a_2/b_2 = 2.58$ (or 14.09) and 3.07 (or 19.78) for prolate and oblate spheroids, respectively. We considered the particles with the following refractive indices of the core and mantle: $\tilde{m}_{\text{core}} = 1.5 + 0.0i$, $1.5 + 0.05i$ and $\tilde{m}_{\text{mantle}} = 1.3 + 0.0i$, $1.3 + 0.05i$. The calculations were performed with a resolution of 0.1–0.2 in size parameter.

A. Nonabsorbing Spheroids

Figures 3 and 4 illustrate the size dependence of the efficiency factors for scattering Q_{sca} for nonabsorbing spheroids with $a_1/b_1 = 2$ and $\alpha = 0°$. Three values of the volume ratio $V_{\text{core}}/V_{\text{mantle}} = 0$, 0.5, and 1.0 are considered in which two extreme cases represent the homogeneous spheroids consisting of mantle and core

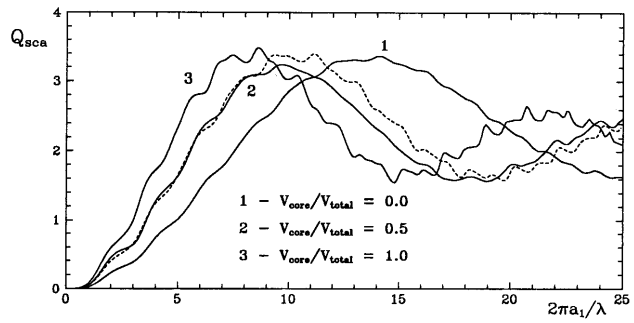

Fig. 4. Same as Fig. 3 but for oblate spheroids.

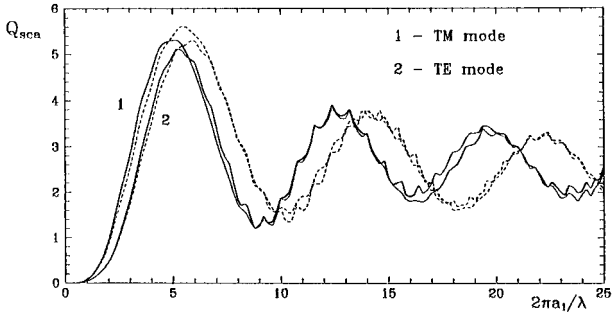

Fig. 6. Same as Fig. 5 but for oblate spheroids.

materials. The large-scale behavior of the curves in Figs. 3 and 4 is a result of the interaction between incident radiation and the radiation that passes through the particle. Because of the interference, one can obtain a series of maxima and minima usually with decreasing amplitude. For coated spheroids, the qualitative explanation of such oscillations remains similar to that for homogeneous spheroids (see Ref. 24). The large-scale phenomena are roughly described by an anomalous diffraction approximation: the maxima height depends on the particle shape and the refractive index whereas their position can be determined by the phase shift of the central ray equal to $\rho = 4\pi/\lambda(l_{core}|\tilde{m}_{core} - 1| + l_{mantle}|\tilde{m}_{mantle} - 1|)$, where $2l_{core}$ and $2l_{mantle}$ are the ray paths in the core and mantle, respectively. The oscillation period can be obtained from the solution to $\rho = 2\pi$. A similar explanation is also valid at oblique incidence as seen from Figs. 5 and 6. The small deviations of the period from that predicted by anomalous diffraction can be explained by the edge phenomena.

It was also found that the curves for oblate spheroids at parallel incidence resemble those for prolate particles at perpendicular incidence and vice versa (Ref. 24). A comparison of Figs. 3 and 5 and Figs. 4 and 6 gives evidence that this is typical for coated spheroids as well. Note that the positions of first maxima for prolate spheroids with $a_1/b_1 \geq 2$ are approximately the same when we consider the factors as a function of parameter x_v.

For a core–mantle particle, it is possible to introduce the effective refractive index $\tilde{m}_{eff}$ that can be defined as a volume-averaged refractive index $\tilde{m}_{eff} = (\tilde{m}_{core}V_{core} + \tilde{m}_{mantle}V_{mantle})/V_{total}$. Then we obtain $\tilde{m}_{eff} = 1.4$ for the cases shown in Figs. 3–6. The corresponding curves that were calculated for homogeneous spheroids are plotted in Figs. 3–6 by the dashed curves, indicating a good correspondence of scattering factors for effective and coated particles to a first maximum.

The curves of the efficiency factors for oblate particles show the small-scale ripples superimposed on the major oscillations. These ripplelike fluctuations result from the resonances of virtual modes[27] and are much more obvious for oblate particles than for prolate particles.

From Fig. 7, where the efficiency factors for elongated and flat particles are plotted, it can be seen that the values of Q_{sca} for prolate and oblate spheroids differ strongly at parallel incidence. At perpendicular incidence, the behavior of the factors resembles the results presented in Figs. 3–6. However, the difference between prolate and oblate spheroids is greater. If we consider the cross sections instead of the efficiency factors, the values of C_{sca} between $a_1/b_1 = 2$ and 10 differ by a smaller amount than those shown in Figs. 3, 4, and 7. This can be explained by

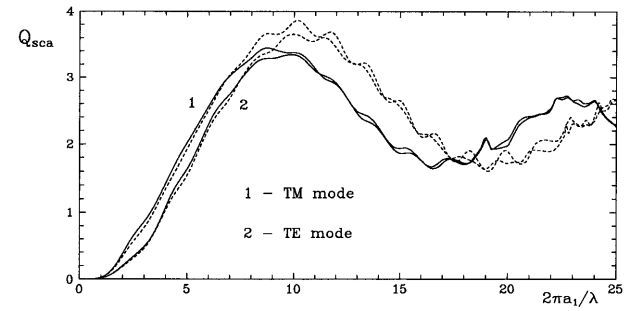

Fig. 5. Scattering efficiency factors Q_{sca} at $\alpha = 90°$ as a function of size parameter $2\pi a_1/\lambda$ for the prolate coated spheroids (solid curves): $\tilde{m}_{core} = 1.5 + 0.0i$, $\tilde{m}_{mantle} = 1.3 + 0.0i$, $a_1/b_1 = 2$. The dashed curve represents the results for homogeneous spheroids with $\tilde{m} = 1.4 + 0.0i$.

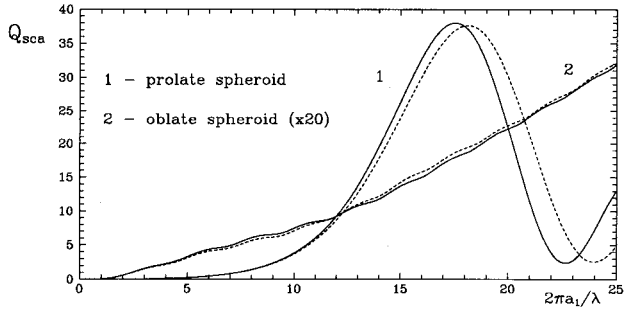

Fig. 7. Scattering efficiency factors Q_{sca} at $\alpha = 0°$ as a function of size parameter $2\pi a_1/\lambda$ for the coated spheroids (solid curves): $\tilde{m}_{core} = 1.5 + 0.0i$, $\tilde{m}_{mantle} = 1.3 + 0.0i$, $a_1/b_1 = 10$. The dashed curves represent the results for homogeneous spheroids with $\tilde{m} = 1.4 + 0.0i$. The factors for oblate spheroids were multiplied by 20.

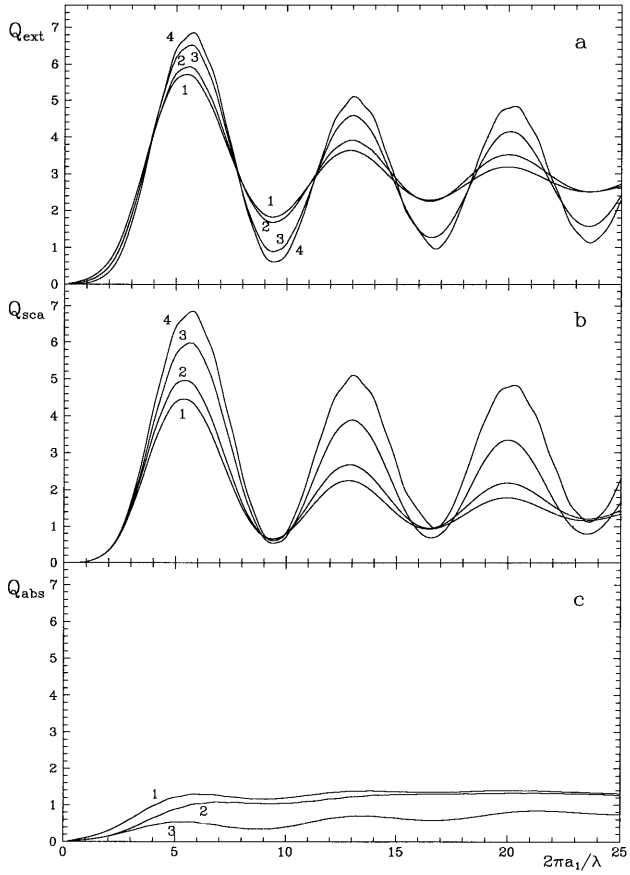

Fig. 8. Efficiency factors for a, extinction Q_{ext}; b, scattering Q_{sca}; and c, absorption Q_{abs} at $\alpha = 0°$ as a function of size parameter $2\pi a_1/\lambda$ for the prolate coated spheroids: $a_1/b_1 = 2$; 1, $\tilde{m}_{core} = 1.5 + 0.05i$, $\tilde{m}_{mantle} = 1.3 + 0.05i$; 2, $\tilde{m}_{core} = 1.5 + 0.05i$, $\tilde{m}_{mantle} = 1.3 + 0.0i$; 3, $\tilde{m}_{core} = 1.5 + 0.0i$, $\tilde{m}_{mantle} = 1.3 + 0.05i$; 4, $\tilde{m}_{core} = 1.5 + 0.0i$, $\tilde{m}_{mantle} = 1.3 + 0.0i$.

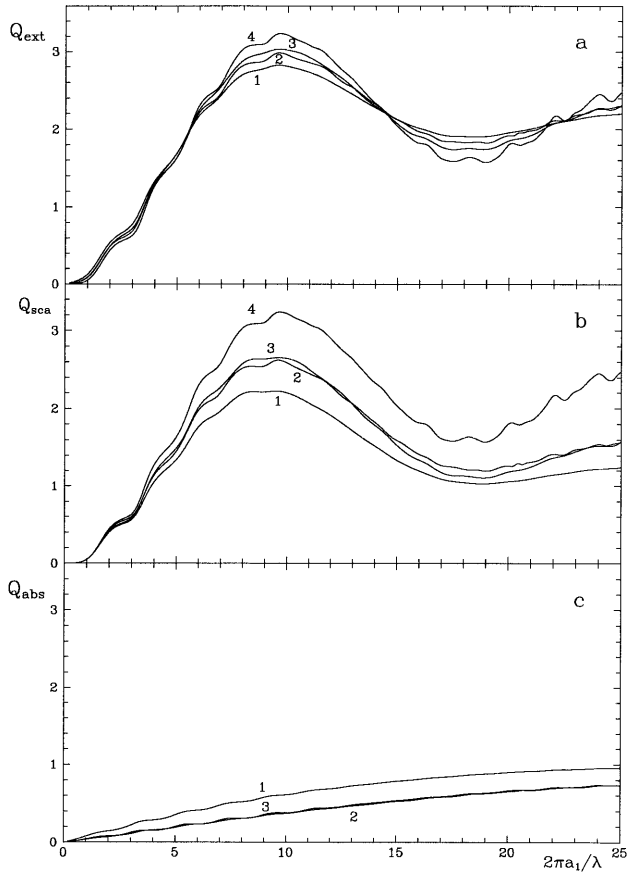

Fig. 9. Same as Fig. 8 but for oblate spheroids.

the large difference in geometric cross sections $G(\alpha)$ [see Eqs. (48) and (49)].

B. Absorbing Spheroids

Figures 8 and 9 demonstrate how the absorption in core or (and) mantle influences the optical properties of prolate and oblate spheroids at parallel incidence. The general behavior of extinction factors for spheroids is similar to that for coated spheres: the damping of the interference and ripplelike structure and the convergence of efficiency factors to the limit of geometrical optics ($Q_{ext} \to 2$, $Q_{sca} \to 1$, $Q_{abs} \to 1$) can be seen when the absorption grows. Note that the absorption in core or (and) mantle causes a decrease of the height of maxima but acts weakly on their position because of the same phase shift of the central ray. However, because of different mantle thicknesses [as follows from Eqs. (62) and (63), $(a_1 - a_2)/a_1 \approx 0.05$, and $(b_1 - b_2)/b_1 \approx 0.4$ for prolate and oblate spheroids, respectively], the presence of an absorbing core or mantle gives distinct results (curves 2 and 3 in Figs. 8 and 9).

It is interesting to note that, for $2\pi a_1/\lambda \geq 16$, the prolate coated spheroid with a dielectric mantle (curve 2 in Fig. 8) absorbs approximately as much radiation as that composed of the absorbing core and absorbing mantle. This phenomenon is due to the inhomogeneity of the particle: the nonabsorbing mantle refracts the incident light, concentrates it on the absorbing core, and, thus, the total absorption efficiency increases.

In the case of the nonabsorbing core and absorbing mantle, the latter screens the core that leads the optical properties of particles closer to those of the dielectric particles than to the highly absorbing ones but with a damped ripplelike structure.

For the oblate coated particles considered, the absorption in core and mantle produces similar effects in extinction, scattering, and absorption (see curves 2 and 3 in Fig. 9). It is also seen that the ripplelike structure is attributed mainly to the dielectric mantle because it is generated by the resonances of virtual modes damped in the absorbing particles.[27]

Appendix

The expressions for integrals of products of normalized angular spheroidal functions $\bar{S}_{ml}(c, \eta) = N_{ml}^{-1}(c) S_{ml}(c, \eta)$ and their first derivatives $\bar{S}'_{ml}(c, \eta) = N_{ml}^{-1}(c) S'_{ml}(c, \eta)$ can be represented as a series containing the expansion coefficients d_r^{ml} of prolate

angular spheroidal functions in terms of associated Legendre functions (Ref. 21):

$$\delta_{nl}^{(m)}(c_i, c_j) = \int_{-1}^{1} \bar{S}_{mn}(c_i, \eta)\bar{S}_{ml}(c_j, \eta)\mathrm{d}\eta$$
$$= N_{mn}^{-1}(c_i)N_{ml}^{-1}(c_j) \sum_{r=0,1}^{\infty}{}' d_r^{mn}(c_i)d_r^{ml}(c_j) \times \frac{2}{2r+2m+1}\frac{(r+2m)!}{r!},$$

$$\gamma_{nl}^{(m)}(c_i, c_j) = \int_{-1}^{1} \bar{S}_{mn}(c_i, \eta)\bar{S}_{ml}(c_j, \eta)\eta\mathrm{d}\eta$$
$$= N_{mn}^{-1}(c_i)N_{ml}^{-1}(c_j) \sum_{r=0,1}^{\infty}{}' d_r^{mn}(c_i) \times \left[d_{r-1}^{ml}(c_j) \frac{r}{2r+2m-1} + d_{r+1}^{ml}(c_j) \frac{r+2m+1}{2r+2m+3} \right] \times \frac{2}{2r+2m+1}\frac{(r+2m)!}{r!},$$

$$\kappa_{nl}^{(m)}(c_i, c_j) = \int_{-1}^{1} \bar{S}'_{mn}(c_i, \eta)\bar{S}_{ml}(c_j, \eta)(1-\eta^2)\mathrm{d}\eta$$
$$= N_{mn}^{-1}(c_i)N_{ml}^{-1}(c_j) \sum_{r=0,1}^{\infty}{}' d_r^{mn}(c_i) \times \left[d_{r-1}^{ml}(c_j) \frac{r(r+2m+1)}{2r+2m-1} - d_{r+1}^{ml}(c_j) \frac{(r+m)(r+2m+1)}{2r+2m+3} \right] \times \frac{2}{2r+2m+1}\frac{(r+2m)!}{r!},$$

$$\sigma_{nl}^{(m)}(c_i, c_j) = \int_{-1}^{1} [\eta\bar{S}_{mn}(c_i, \eta)]'\bar{S}_{ml}(c_j, \eta)(1-\eta^2)\mathrm{d}\eta$$
$$= N_{mn}^{-1}(c_i)N_{ml}^{-1}(c_j) \sum_{r=0,1}^{\infty}{}' d_r^{mn}(c_i) \times \left[d_{r-2}^{ml}(c_j) \frac{(r-1)r(r+m)}{(2r+2m-3)(2r+2m-1)} + d_r^{ml}(c_j) \frac{3(r+m)(r+m+1)-m^2-2}{(2r+2m-1)(2r+2m+3)} - d_{r+2}^{ml}(c_j) \times \frac{(r+m+1)(r+2m+1)(r+2m+2)}{(2r+2m+3)(2r+2m+5)} \right] \times \frac{2}{2r+2m+1}\frac{(r+2m)!}{r!},$$

$$\omega_{nl}^{(m)}(c_i, c_j) = \int_{-1}^{1} \bar{S}_{mn}(c_i, \eta)\bar{S}_{ml}(c_j, \eta)(1-\eta^2)\mathrm{d}\eta$$
$$= N_{mn}^{-1}(c_i)N_{ml}^{-1}(c_j) \sum_{r=0,1}^{\infty}{}' d_r^{mn}(c_i) \times \left[d_{r-2}^{ml}(c_j) \frac{r(r-1)}{(2r+2m-3)(2r+2m-1)} - d_r^{ml}(c_j) \frac{2[(r+m)(r+m+1)+m^2-1]}{(2r+2m-1)(2r+2m+3)} + d_{r+2}^{ml}(c_j) \frac{(r+2m+1)(r+2m+2)}{(2r+2m+3)(2r+2m+5)} \right] \times \frac{2}{2r+2m+1}\frac{(r+2m)!}{r!},$$

$$\tau_{nl}^{(m)}(c_i, c_j) = \int_{-1}^{1} \left[\bar{S}'_{mn}(c_i, \eta)\bar{S}'_{ml}(c_j, \eta)(1-\eta^2) + \frac{m^2\bar{S}_{mn}(c_i, \eta)\bar{S}_{ml}(c_j, \eta)}{1-\eta^2} \right]\mathrm{d}\eta$$
$$= N_{mn}^{-1}(c_i)N_{ml}^{-1}(c_j) \sum_{r=0,1}^{\infty}{}' d_r^{mn}(c_i)d_r^{ml}(c_j) \times \frac{2(r+m)(r+m+1)}{2r+2m+1}\frac{(r+2m)!}{r!}.$$

The prime over the summations indicates that the even (odd) terms only are summarized when the index $(n-m)$ is even (odd).

To check the calculations we can use the rule that the simultaneous replacements of n by l and c_i by c_j in integrals δ_{nl}, γ_{nl}, ω_{nl}, and τ_{nl} should not change them, i.e., $\delta_{nl}^{(m)}(c_i, c_j) = \delta_{ln}^{(m)}(c_j, c_i)$, etc. The relations between integrals also exist:

$$\kappa_{nl}^{(m)}(c_i, c_j) + \kappa_{ln}^{(m)}(c_j, c_i) = 2\gamma_{nl}^{(m)}(c_i, c_j),$$
$$\sigma_{nl}^{(m)}(c_i, c_j) + \sigma_{ln}^{(m)}(c_j, c_i) = 2\delta_{nl}^{(m)}(c_i, c_j) - \omega_{nl}^{(m)}(c_i, c_j).$$

The coefficients d_r^{mn} reach their maximum values for the index $r = n - m$: $d_{n-m}^{mn} \approx 1$; for the indices $r < n - m$ or $r > n - m$ the coefficients d_r^{mn} drop rapidly. Therefore, the integrals (sums) considered converge rapidly. For oblate spheroidal functions the replacements $d_r^{mn}(c) \to d_r^{mn}(-ic)$ and $N_{mn}(c) \to N_{mn}(-ic)$ should be made.

We are grateful to V. B. Il'in and anonymous reviewers for valuable comments. We thank M. I. Mishchenko who brought to our attention the paper of Cooray and Ciric.[15] This research was made possible in part by grant NVT000 from the International Science Foundation. The calculations were carried out mainly on the PC/AT 486 computer, which was purchased with funds from the Fund for East Europe Sponsorship 12161.

References and Notes

1. B. T. Draine, "The discrete-dipole approximation and its application to interstellar graphite grains," Astrophys. J. **333,** 848–872 (1988).
2. J. L. Hage, J. M. Greenberg, and R. T. Wang, "Scattering from arbitrarily shaped particles: theory and experiment," Appl. Opt. **30,** 1141–1152 (1991).
3. B. T. Draine and J. Goodman, "Beyond Clausius–Mossotti: wave propagation on a polarized point lattice and the discrete-dipole approximation," Astrophys. J. **405,** 685–697 (1993); P. J. Flatau, G. L. Stephens, and B. T. Draine, "Light scattering by rectangular solids in the discrete-dipole approximation: a new algorithm exploiting the block-Toeplitz structure," J. Opt. Soc. Am. A **7,** 593–600 (1990); K. Lumme and J. Rahola, "Light scattering by porous dust particles in the discrete-dipole approximation," Astrophys. J. **425,** 653–677 (1994).
4. J. I. Peltoniemi, K. Lumme, K. Muinonen, and W. M. Irwine, "Scattering of light by stochastically rough particles," Appl. Opt. **28,** 4088–4095 (1989).
5. F. Rouleau and P. G. Martin, "A new method to calculate the extinction properties of irregularly shaped particles," Astrophys. J. **414,** 803–814 (1993).
6. G. Mie, "Beiträge zur Optik trüber Medien speziell kolloidaler Metallösungen," Ann. Phys. (Leipzig) **25,** 377–445 (1908).
7. K. S. Shifrin, "Light scattering by core-mantle particles," Izv. Akad. Nauk SSSR Ser. Geofiz. N **2,** 15–21 (1952).
8. A. C. Lind and J. M. Greenberg, "Electromagnetic scattering by obliquely oriented cylinders," J. Appl. Phys. **37,** 3195–3203 (1966).
9. G. A. Shah, "Scattering of plane electromagnetic waves by infinite concentric circular cylinders at oblique incidence," Mon. Not. R. Astron. Soc. **148,** 93–102 (1972).
10. S. Asano and G. Yamamoto, "Light scattering by a spheroidal particle," Appl. Opt. **14,** 29–49 (1975).
11. V. G. Farafonov, "The scattering of a plane electromagnetic wave by a dielectric spheroid," Differential Equations (Sov.) **19,** 1765–1777 (1983).
12. N. V. Voshchinnikov and V. G. Farafonov, "Light scattering by dielectric spheroids. I," Opt. Spektrosk. **58,** 81–85 (1985).
13. N. V. Voshchinnikov and V. G. Farafonov, "Optical properties of spheroidal particles," Astrophys. Space Sci. **204,** 19–86 (1993).
14. T. Onaka, "Light scattering by spheroidal grains," Ann. Tokyo Astron. Obs. **18,** 1–54 (1980).
15. M. F. R. Cooray and I. R. Ciric, "Scattering of electromagnetic waves by a coated dielectric spheroid," J. Electro. Waves Appl. **6,** 1491–1507 (1992).
16. B. P. Sinha and R. H. MacPhie, "Electromagnetic scattering by prolate spheroids for plane waves with arbitrary polarization and angle of incidence," Radio Sci. **12,** 171–184 (1977).
17. B. Peterson and S. Ström, "T-matrix formulation of electromagnetic scattering from multilayered scatters," Phys. Rev. D **10,** 2670–2684 (1974).
18. P. W. Barber, "Scattering and absorption by homogeneous and layered dielectrics," in *Acoustic, Electromagnetic and Elastic Wave Scattering—Focus on the T-Matrix Approach*, V. K. Varadan and V. V. Varadan, eds. (Pergamon, New York, 1980), pp. 191–209; D.-S. Wang and P. W. Barber, "Scattering by inhomogeneous nonspherical objects," Appl. Opt. **18,** 1190–1197 (1979); D.-S. Wang, C. H. Chen, P. W. Barber, and P. J. Wyatt, "Light scattering by polydisperse suspensions of inhomogeneous nonspherical particles," Appl. Opt. **18,** 2672–2678 (1979).
19. V. N. Lopatin and F. Ya. Sid'ko, *Introduction to Optics of Cell Suspension* (Nauka, Novosibirsk, Russia, 1987).
20. C. Flammer, *Spheroidal Wave Functions* (Stanford U. Press, Stanford, Calif., 1957).
21. I. V. Komarov, L. I. Ponomarev, and S. Yu. Slavyanov, *Spheroidal and Coulomb Spheroidal Functions* (Nauka, Moscow, 1976).
22. J. J. Bowman, T. B. A. Senior, and P. L. E. Uslenghi, *Electromagnetic and Acoustic Scattering by Simple Shapes* (North-Holland, Amsterdam, 1969).
23. J. A. Stratton, *Electromagnetic Theory* (McGraw-Hill, New York, 1941).
24. S. Asano, "Light scattering properties of spheroidal particles," Appl. Opt. **18,** 712–723 (1979).
25. P. W. Barber, "Resonance electromagnetic absorption by nonspherical dielectric objects," IEEE Trans. Microwave Theory Tech. **MTT-25,** 373–381 (1977).
26. M. I. Mishchenko and L. D. Travis, "T-matrix computations of light scattering by large spheroidal particles," Opt. Commun. **109,** 16–21 (1994).
27. C. F. Bohren and D. R. Huffman, *Absorption and Scattering of Light by Small Particles* (Wiley, New York, 1983).
28. N. V. Voshchinnikov, "Dust grains in reflection nebulae. Spherical core-mantle grains," Sov. Astron. **22,** 561–566 (1978).
29. The numerical code is available on request from N. V. Voshchinnikov, e-mail: nvv@aispbu.spb.su.